

# Pamukkale Üniversitesi Mühendislik Bilimleri Dergisi

## Pamukkale University Journal of Engineering Sciences



## Examination of 3D printing parameters using machine learning

## Makine öğrenmesi ile 3D yazdırma parametrelerinin incelenmesi

Mehmet Altuğ<sup>1\*</sup>, Yakup Yılmaz<sup>2</sup>

<sup>1</sup>Machine and Metal Technologies, Malatya OIZ Vocational High School, Inonu University, Malatya, Türkiye.

mehmet.altug@inonu.edu.tr

<sup>2</sup>Applied Science Technology, Graduate School Of Natural And Applied Sciences, Inonu University, Malatya, Türkiye yk.yilmaz4448@gmail.com

Received/Geliş Tarihi: 03.05.2025 Accepted/Kabul Tarihi: 27.10.2025 Revision/Düzeltme Tarihi: 17.10.2025 doi: 10.65206/pajes.91679
Research Article/Araştırma Makalesi

#### **Abstract**

In this study, the mechanical properties of tensile samples produced in 3D printers with the fused deposition method (FDM) were investigated. Here, the parameters such as layer (filament) thickness, infill type and support angle in the FDM method were examined. The production was produced with Up-right and edge directions. As a result of the experiments, the best layer thickness in terms of tensile strength was 0.09 mm, and the infill type was full infill type, while different results were obtained in the support angle. According to the variance analysis (ANOVA) values, it was observed that the layer thickness and infill type were quite effective on the tensile strength, but the support angle was at a negligible level. In the second stage, the results were estimated with xgboost and catboost from the machine learning algorithms and linear regression models. The most effective algorithm on the examined mechanical properties was determined as the catboost algorithm.

**Keywords:** Fused deposition model, Mechanical properties, Machine learning, Regression, Prediction.

#### 1 Introduction

Fused Deposition Modeling (FDM) is an additive manufacturing technique that works by stacking layers upon layers of molten material in a heated nozzle to produce a 3D designed part (Fig 1). FDM is one of the most common techniques employed in the field of 3D printing, and it has become one of the popular rapid prototyping techniques in recent years. This is due to its ability to construct functional parts with complex geometric shapes in a short time. The FDM working method is shown in Figure 1.

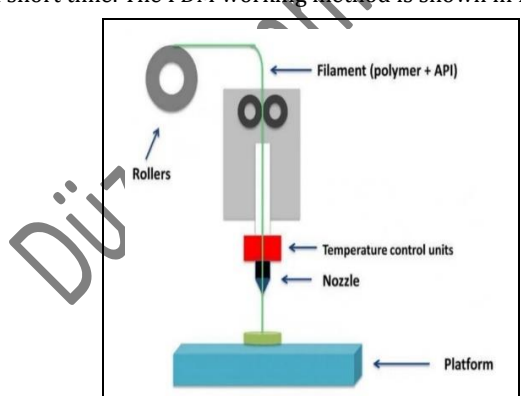


Figure 1. FDM method.

Öz

çalışmada ergiyik etodu vıăma (Fused Deposition Modelleme/FDM) vöntemi zıcılarda üretilen numunelerinin mekanik **\ö**zellikler incelendi. Burada yöntemindeki katman (fila lieh.) kumlığı, dolgu tipi ve support açısı gibi parametreler incelend. Üretim Up-right ve edge yönleri ve her bir yön için Taguchi L25 kerzy tasarımıyla üretildi. Deneyler neticesinde çekme mukavemeti tasısında en iyi katman kalınlığı 0,09 mm, dolgu tipi olarak full dolgu tipi olurken support açısında farklı sonuçlar elde . no. lizi (ANOVA) değerlerine göre parametrelerden edildi. Varyans katman ka mlığı ve dolgu tipinin çekme mukavemeti üzerinde oldukça etkili olduğu ancak support açısının göz ardı edilebilecek düzeyde olduğı gözlemlendi. İkinci aşamada sonuçlar makine öğrenmesi algoritmularından xgboost ve catboost ile ve linear regression ile tarmin modelleri yapıldı. İncelenen mekanik özellikler üzerinde en etkin algoritma catboost algoritması olarak belirlendi.

**Anahtar kelimeler:** Ergiyik yığma metodu, Mekanik özellikler, Makine öğrenmesi, Regresyon, Tahmin.

Cantre et al. conducted studies on the positioning of Acrylonitrile Butadiene Styrene-ABS and polycarbonate parts during 3D software. In these studies, they obtained up to 33% differences in the mechanical properties of ABS parts and 20% differences in the mechanical properties of polycarbonate parts [1]

Sood et al. examined the effects of parameters such as layer thickness and support angle on the mechanical properties of 3D models produced by FDM method. In their study, they concluded that layer thickness and scanning direction change the temperature of the bonds between the layers and therefore have an effect on strength [2].

Tekinalp et al. compared the mechanical properties of reinforced ABS materials and conventional composites. Here, the tensile strength and modulus of 3D specimens were increased by  $\sim 115\%$  and  $\sim 700\%$ , respectively [3].

Ning et al. produced carbon fiber reinforced plastic composite parts by FDM method and investigated their tensile strength. In their study, they stated that the best layer thickness for tensile and yield strength is 0.15 mm and 0.25 mm layer thickness is ideal for hardness and ductility [4].

Sa'ude et al. investigated the mechanical properties of ABS materials containing copper powders produced by FDM method. In their study, they observed that up to 22% copper

<sup>\*</sup>Corresponding author/Yazışılan Yazar

powder reinforcement significantly affected the mechanical properties [5].

Bacak et al. were trying to work out what the process parameters were doing to the tensile strength of the PLA samples made using the FDM method on a 3D printer. In their study, they obtained higher tensile stress at 100% filling rate compared to 20% filling rate [6].

Evlen, aimed to investigate the effects of occupancy rate on mechanical properties in three-dimensional printers. They observed that the values of roughness and tensile strength were opposite to those of 10% and 20% occupancy rate after 30% occupancy rate [7].

The process parameters for tensile strength were optimised by applying Taguchi methodology. Following a thorough review of the data, it was determined that the most effective parameter on tensile strength was the fill rate. Research has identified the scanning angle and print speed as the other significant parameters [8].

It is imperative that improvements are made in order to meet the mechanical requirements of the load-bearing components. The study concluded that the addition of 6 mm-long carbon fibre reinforcement to the structure can lead to a substantial enhancement in part strength. Furthermore, it was determined that the printing pattern has a considerable impact on the mechanical properties of the structure [9].

It was determined through a combination of measurement results and Taguchi analysis that an increase in nozzle diameter resulted in an increase in the hardness value of the sample. Conversely, the lowest values were observed in productions made with a nozzle diameter of 0.25 mm, as well as incomplete adhesion. The layer height is another effective parameter, with a 9.52% impact. The statistical significance of both parameters was confirmed by analysis of variance, which also demonstrated that the effects of nozzle angle and nozzle temperature were minimal. It was established that the printing parameters which yielded the highest hardness value within the specified ranges were as follows: a nozzle diameter of 0.6 mm, a layer height of 0.1 mm, a nozzle angle of 30°, and a nozzle temperature of 210°C [10].

Here, parameters such as layer (filament) thickness, filler type and support angle in the FDM method were examined. Production was performed with up-right and edge orientations. Analysis of variance (ANOVA) was performed. In the second stage, the results were predicted by machine learning algorithms xgboost and Catboost and linear regression.

### 2 Material and method

This technology is employed in the field of three-dimensional (3D) printing to manufacture robust, durable, and dimensionally stable components that exhibit both dimensional accuracy and repeatability. The present study investigates the mechanical properties of prototypes (tensile specimens) produced by 3D printers utilising the FDM method. Flow chart of this study is shown in Figure 2.

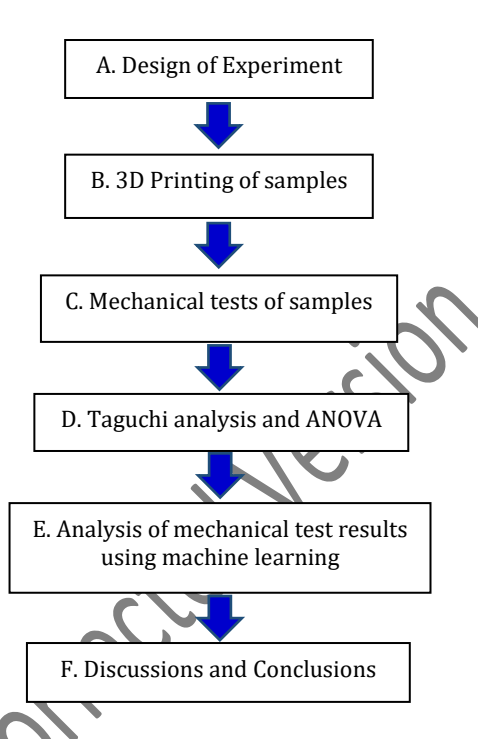


Figure 2. Flowchart of this study

Here, parameters such as layer (filament) thickness, filler type and support angle in the FDM method were controlled by Taguchi  $L_{25}$  experimental design and 25 specimens were produced in the edge and up-right directions (Figure 5). The specimens of this study were produced on Zortrax M200 model 3D printers (Figure 3). Z-ultrate series ABS filament was used as the material. The specimens were dimensionally prepared for tensile testing based on ASTM D638 standard with dimensions of  $165 \times 19 \times 3.2$  mm (Figure 4). Up-right and edge positioning is given (Figure 4). 3D parameters and levels are given in Table 1 and fill type is given in Figure 6. The MTS EM tensile device was used to perform this test. The results were analyzed and plotted in Minitab 21 program.



Figure 3. 3D printer.

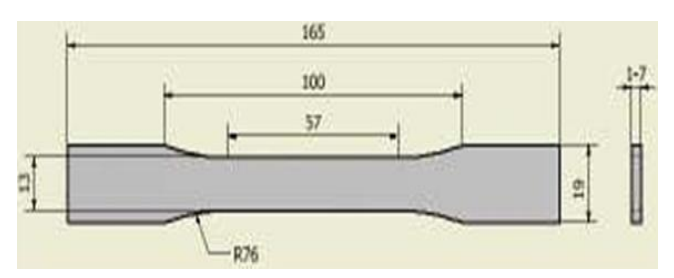


Figure 4. Tensile sample dimensions.

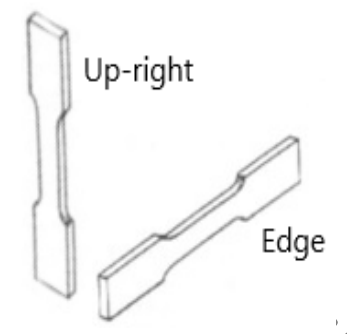


Figure 5. Up-right and edge.

Table 1. 3D print parameters and levels.

3D parameters		]	Levels		1
	1	2	3	4	5
Build direction	Edge	Up-right	-	* 6)	<b>.</b> .
Layer thickness (mm)	0.09	0.14	0.19	0.29	0.39
Infill type	Full	Light	Medium	Mesh	Solid
Support angle (°)	20	30	40	50	60



Figure 6.3D print infill type.

#### 2.1 Optimization with machine learning

#### 2.1.1 CatBoost (categorical boosting)

CatBoost is a gradient boosting algorithm that has been specifically developed for the handling of categorical features. CatBoost represents a departure from conventional methodologies that employ one-hot encoding. Instead, it introduces a novel approach that aims to minimise overfitting and reduce computational complexity [11]. The system has been developed to construct decision trees in an optimal manner, utilising both categorical and continuous features. In a manner analogous to other gradient boosting methods,

$$J = \frac{1}{|S_j|} \sum_{x_i \in S_j}^n y_i \tag{1}$$

The location is as follows:

 $S_i$  denotes the set of observations relevant to category  $C_i$ .

After the categorical features have been transformed, the model then builds decision trees in a way that's similar to standard gradient boosting. The idea behind each decision tree is to reduce the remaining error from the former model.

$$L_t = \sum_{i=1}^{N} [y_i - f_{t-1}(x_i) - \eta h_t(x_i)]^2$$
 (2)

CatBoost employs an iterative process to incorporate decision trees that have been trained on residuals [11]–[13]. The model under consideration has been developed for the purpose of handling categorical variables by means of ordered target statistics. The way these statistics work out target values is by looking at past data points, not all data points together. This stops the problem of overfitting. The dataset X is defined by the target variable Y, with the i-th observation represented by xi and the categorical feature Cj. The calculation of the key transformation for a categorical feature is outlined as follows:

 $\hat{C}j$  signifies the average target value for the categorical feature.

This transformation is achieved through the utilisation of ordered goal statistics. In this process, the goal statistic is computed for each data point using only preceding data points. This process is known as the 'exclusion of data leakage' [11]–[13].

#### The location is as follows:

The abbreviation  $f_{t-1}(x_i)$  denotes the prediction of the previous model, whilst  $\eta$  is the learning rate. is employed to denote the decision tree model that has been trained on the residuals. The objective of each tree is to minimise this residual error, with the effect of each tree being adjusted using the gradient descent method. Subsequent to the construction of the

trees, the last model, f(x), is constituted as a weighted sum of all the decision trees. The learning rate  $(\eta)$  is a critical factor in the training process, as it determines the importance or weight assigned to each tree in the learning process [11]–[13].

$$f(x) = f_0(x) + \sum_{t=1}^{T} \eta h_t(x)$$
 (3)

In the initial model, designated  $f_0(x)$ , the mean of the goal values is typically employed. The objective function employed for the optimisation of the CatBoost model is analogous to that utilised in other gradient boosting algorithms. The following illustration is offered in order to elucidate the aforementioned point. For this purpose, the loss function for regression will be considered, i.e. the mean squared error (MSE)[11]–[13].

$$\mathcal{L}(\theta) = \sum_{i=1}^{N} (y_i - f(x_i))^2 \tag{4}$$

The gradient of this loss function is used to help the model improve. In machine learning, the new tree (ht(x)) is adjusted at each step to match the negative gradient of the loss function. This is congruent with the residuals from the preceding model.

CatBoost also uses regularization techniques to stop overfitting. The model we're talking about uses a mix of features and techniques to improve how well the model generalises. In order to achieve this objective, an exploration is undertaken of a variety of methodologies for combining features [11]–[13]. The regularization term can be expressed as follows:

$$\Omega(h_t) = \gamma T + \frac{1}{2}\lambda \sum_{j=1}^{T} (\omega_j)^2$$
 (5)

The location is as follows:

T is the number of leaves in the tree,

 $\omega_i$  is the weight of each leaf node,

It is evident that both  $\gamma$  and  $\lambda$  function as regularization parameters, thereby exerting a degree of control over the complexity of the trees.

In the field of polymer research, CatBoost is great for working with complex data sets that include both categories and continuous variables. To show this, think about a study of polymer materials. In this study, the conditions during the polymerisation process (e.g. temperature, pressure, and types of catalyst) can be put into groups. At the same time, properties such as tensile strength, viscosity, and melting temperature are continuous variables. CatBoost has been shown to be good at dealing with different types of data. You can build strong predictive models without having to do a lot of preparation or creating features [11]–[13].

To illustrate this point, consider the task of predicting the tensile strength of a polymer. This can be achieved through the consideration of various processing conditions and chemical additives:

$$\hat{y}_i = f(x_i) = f_0(x_i) + \sum_{t=1}^{T} \eta h_t(x_i)$$
 (6)

In this study, the dependent variable is represented by Y\_i, which is the predicted tensile strength. The independent variables are represented by X\_i, which includes both continuous features (e.g. temperature) and categorical features (e.g. the type of chemical additive).

CatBoost has been shown to be effective in handling categorical features directly, thus obviating the necessity for one-hot encoding. This property has been demonstrated to reduce computational complexity, enhancing the model's efficiency and accuracy. Consequently, CatBoost is well-suited for polymer field tasks involving substantial and intricate datasets.

# 2.1.2 XGBoost (eXtreme gradient boosting)

XGBoost is an improved version of the gradient boosting algorithm. It has been designed to make training more efficient, improve prediction accuracy and make models easier to understand. Using regularisation techniques is important for preventing overfitting. It also helps to manage data that is incomplete and use more efficient training methods, such as parallelisation and hardware optimisations [11], [14]. XGBoost constructs models by sequentially integrating decision trees, with each tree being calibrated to the residuals (errors) from the preceding model. In essence, the objective is to minimise the loss function by incorporating an additional regularisation term. That II help stop overfitting.

At the t-th iteration, the model is updated as follows:

$$L_{t} = \sum_{i=1}^{N} [y_{i} - f_{t-1}(x_{i}) - \eta h_{t}(x_{i})]^{2}$$
 (7)

The location is as follows:

For instance, the true label for i is denoted by y\_i. To illustrate, within a decision tree,  $f_-(t-1)$  (x\_i) denotes the model's prediction for instance i at the preceding step,  $h_-t$  (x\_i) signifies the prediction of the new decision tree at the  $t^-(th)$  step, and  $\eta$  denotes the learning rate [11]. This formula is employed to minimise the residual error from the preceding model. The ultimate model prediction is the aggregate of all tree predictions. XGBoost basically penalises complexity and reduces overfitting by using regularisation [15]. We include the regularisation term  $\Omega(f)$  in The objective function is defined as follows to keep the model's complexity in check.

$$\Omega(f) = \gamma T + \frac{1}{2}\lambda \sum_{i=1}^{T} (\omega_i)^2$$
 (8)

The location is as follows:

It can thus be concluded that T denotes the total number of leaves in the tree,  $w_{-j}$  denotes the weight of the j-th leaf, and  $\gamma$  is a regularisation parameter that controls the number of leaves in the tree. In addition, there is another regularisation parameter, denoted by  $\lambda$ , that controls the size of the weights [11].

The regularization term has been demonstrated to function as a mechanism that discourages the development of overly complex trees with numerous leaves and substantial weights, thereby aiding in the process of preventing overfitting [16].

The last thing we need to do to minimise the objective function in XGBoost is combine the loss function (residuals) and the regularisation term:

$$\mathcal{L}(f) = \sum_{i=1}^{N} L(y_i, f(x_i) + \Omega(f))$$
 (9)

The location is as follows:

The loss function  $L(y_i, f(x_i))$ , which is employed to quantify the discrepancy between the true label yi and the predicted value f(xi), is a fundamental component of the model. The regularization term  $\Omega(f)$ , which was previously defined, plays a crucial role in ensuring the stability and accuracy of the model. The objective of XGBoost is to identify the function f(x) that minimises the objective function [11].

XGBoost constructs trees by employing a greedy algorithm that selects the optimal split at each node, as determined by the objective function. The optimal split Q for a given node can be determined by maximising the gain:

Gain (q) = 
$$\frac{1}{2} \left( \frac{(\Sigma_{i \in L} g_i)^2}{h_L + \lambda} + \frac{(\Sigma_{i \in R} g_i)^2}{h_R + \lambda} - \frac{(\Sigma_{i \in S} g_i)^2}{h_S + \lambda} \right)$$
 (10)

The location is as follows:

It is evident that 'gi' and 'hi' represent the gradient and Hessian of the loss function, respectively, i.e. the first and second derivatives. Furthermore, 'L', 'R', and 'S' denote the left, right, and split node, in that order [11].

The gain is defined as the reduction in loss following the implementation of the split. It is important to note that the objective of the split is to maximise the gain [17].

The final prediction is derived from the summation of the predictions of all individual trees once they have been constructed.

$$f(x) = f_0(x) + \sum_{t=1}^{T} \eta h_t(x)$$
 (11)

The location is as follows:

The initial model, designated  $f_0(x)$ , is frequently the mean value of the target. The learning rate is denoted by  $\eta$ , and the prediction from the t-th tree is represented by ht(x).

So, the prediction for a new instance is worked out by adding together the predictions of all the trees, with the weights based on the learning rate [18]. XGBoost is a machine learning algorithm that incorporates early stopping as a means of preventing overfitting [19]. During the training phase, the model checks how well it is performing on a separate set of data after each boosting round. If the performance on the validation set doesn't get better after a set number of rounds (called the early stopping round'), the training is stopped [11], [18], [19].

XGBoost has been shown to be a useful tool for predicting polymer properties, especially when numerical and categorical features are both present. When researchers study polymers, they often work with large sets of data. These data include numbers (for example, how thick a liquid is, how strong it is, and what its heat properties are) and categories (for example, the type of polymer, the catalyst used, and the conditions of the reaction). XGBoost is particularly good at making these types of predictions because it can process both numerical and categorical data, and it learns quickly [11]. For instance, Ueki et al. [20] used machine learning (ML) to predict how much we could graft in a radiation-induced graft polymerisation of methacrylate ester monomers onto PE-coated PP fabric. The XGBoost model was the best at predicting what would happen,

and it showed that monomer polarizability and 02 NMR shift were the main things affecting grafting efficiency.

$$\hat{y}_i = f(x_i) = f_0(x_i) + \sum_{t=1}^{T} \eta h_t(x_i)$$
 (12)

To illustrate this point, consider the potential of XGBoost in predicting the stability of a polymer under various conditions. These conditions may include exposure to UV radiation or chemical reactions, with the relevant features being molecular structure, temperature, and the type of additives utilised [11]. The ultimate prediction for polymer property  $\hat{y_i}$  can be expressed as follows.

Çevik et al. investigated the optimisation of parameters in the micro-milling of aluminium alloy produced by additive manufacturing. Here, they used algorithms such as random forest regressor (RFR), gradient boosting regressor (GBR), LightGBM, CatBoost, and k-nearest neighbours (KNN). However, they obtained the best values with CatBoost [21]. Wang et al. 2024 studies the XGBoost algorithm and Lasers Additive Manufacturing (LAM), optimizes and designs traditional processes to obtain a more ideal process flow. This study utilizes the XGBoost algorithm to improve the LAM process, promoting the development of the manufacturing industry and improving the quality and production efficiency of parts [22]. Wang et al. 2022, propose a data-driven failure prediction system framework for metal additive manufacturing equipment to overcome the complexity of failure modelling and the limitations of health monitoring tools. In the proposed failure modelling method, the modelling method based on the XGBoost algorithm shows that the higher the depth value of the tree used, the faster the iterative convergence speed. Compared with other algorithms, the XGBoost-based modelling method can provide higher prediction accuracy [23]. In 3D printing, determining optimal printing parameters remains a challenge and increases pre-printing processing time and material waste. Dabbagh et al. presented the first integration of ML and 3D printing for optimising printing parameters through an easyto-use graphical user interface (GUI) [24]. Zhu et al. developed three ML models, SVR, extreme gradient boosting (XGBoost), and BPNN, to predict melt pool shapes. They measured 210 melt pool parameters as training and testing datasets. The SVR model achieved an accuracy of approximately 93% in predicting melt pool height, while the XGBoost model attained accuracies of 97% and 96.3% in predicting melt pool width and depth, respectively. After optimization, all three models exhibited excellent generalization performance on new sample data [25]. Zhang et al. studied two machine learning algorithms. including XGBoost and Long short-term memory (LSTM). The central hypothesis is that, under various process conditions, machine learning can forecast the melt pool temperature during DED with high accuracy. Four separate instances were used to assess the performance of two machine learning algorithms, including XGBoost and LSTM. However, the performance of the two ML models based on time series does not achieve high accuracy [26]. Huang et al. proposed an artificial intelligence-based printing path optimization design method to provide new ideas and directions for the development of modern printing industry [27]. Zhang et al. provided a comprehensive review of parameter optimization and in-situ monitoring in laser powder bed fusion (L-PBF) technology. They effectively improved the quality of part

manufacturing by deeply extracting the intrinsic links between process parameters and key elements such as melt pool characteristics, porosity, and mechanical properties [28].

Additionally, Veeman et al. investigated layer thickness, filling density, and print direction in FDM using decision trees (DT), random forest (RF) and Adaboost algorithms [29]. Garg and Tai, investigated layer thickness, grid angle, grid width, and print direction in FDM using artificial neural network (ANN) [30]. Agarwal et al. İnvestigated fill percentage, layer height and filling mode in FDM using K-nearest neighbors (KNN), support vector regression (SVR), DT and RF [31]. Zhu et al. İnvestigated layer height, scanning speed, material flow rate and nozzle temperature in FDM using Gradient boosting decision tree (GBDT) [32]. Barrios and Romeo investigated layer height, extrusion temperature and print speed in FDM using RF and DT [33]. Nagarajan et al. investigated angle of deposition in FDM using ANN [34]. Li et al., investigated layer height, printing temperature and print speed in FDM using Adaboost and SVR [35]. Hooda et al. investigated angle of deposition in FDM using RF [36]. Douard et al., investigated support angle and support density in Electron Beam Melting (EBM) using DT [37].

Machine learning methods have become a widely used tool in the health sector for data analysis and diagnosis of diseases and for solving complex problems. In this study, After the experimental parts of the study were completed, optimization was performed with machine learning according to the limited number of experiments and results available. Linear regression, Xgboost and Catboost algorithms were used. The

present study employed Python as the designated programming language. The parameters used are given in the table below. 80% of the data was used for training, while 20% was used for testing.

Table 2 Machine learning parameters

Parameters	Xgboost	Catboost
Learning rate	0,05	0,05
N_estimatör	1000	-
Iteration	-	1000
Eval metric	RMSE	RMSE 💉
Max depth	6	6
Eta	0,3	
Gama	0	361
Border count	-	254
Subsample	1	1

## 3 Results and discussions

The data obtained as a result of tensile tests are given in Table 3. In the table, the tensile force value, the time for the maximum value and the amount of elongation occurring in the specimens are given. In addition, the images of the specimens fractured as a result of the tensile test are given in Figure 7. In this context, Figure 8 shows that the best tensile strength results were obtained at 0.09 mm layer thickness, full filling type and 20° support angle.

Table 3. Design of experiment and results.

Build Direction	Sample	Layer Thickness (mm)	Infill type	Support angle (°)	Y1 Max Force (N)	Y2 Elongation at break (ε)	Υ3 Tensile strength (σ)	Y4 Elastic Module
	1	0.09	Føll	20	376.8948	0.0412	19.32	432.025
	2	0.09	Solid	30	348.3393	0.0393	17.86	584.370
Edge	3	0.09	Medium	40	426.9743	0.0571	21.89	500.850
		7						
		0)						
		4						
Up-right	48	0.39	Medium	30	73.79607	0.059	3.78	180.270
-	<b>4</b> 9	0.39	Light	40	103.8705	0.0827	5.32	126.060
Q	50	0.39	Mesh	50	26.48006	0.0075	1.35	246.068



Figure 7. Specimens fractured after tensile test.

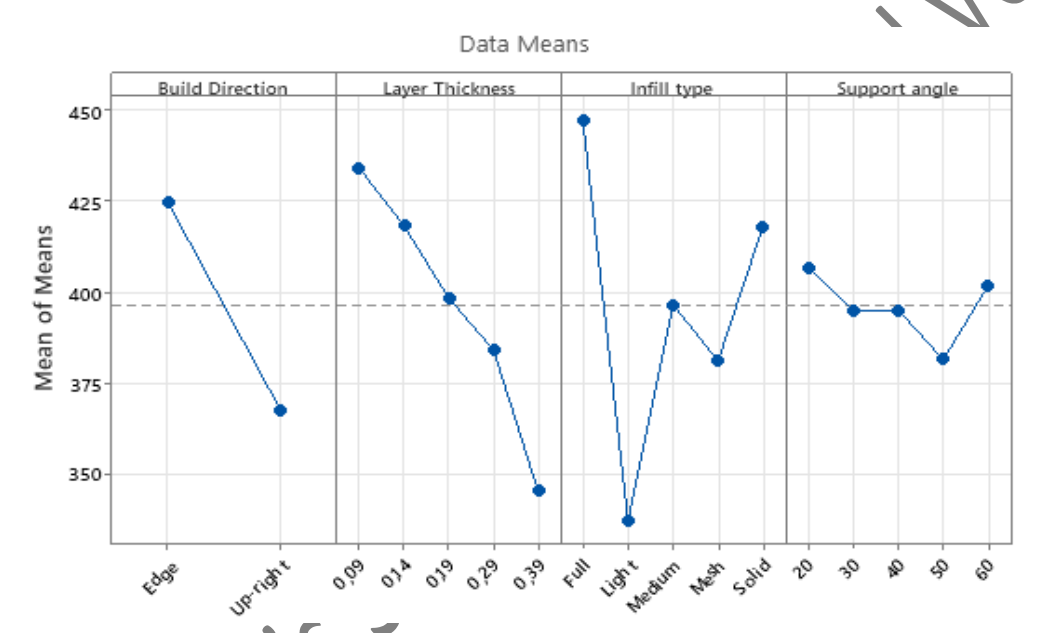


Figure 8. The effects of parameters on max force.

It was also observed that the weakest tensile strength values were obtained at 0.39 mm layer thickness, mesh infill type and  $50^{\circ}$  support angle. When the ANOVA values given for Max Force (Table 4) are analyzed, build direction with 21.87%, Layer thickness with 24.94% and Infill type with 36.43% were effective. However, support angle (1.94%) did not show a significant effect on max force.

symbol DF Seq SS Contribution Adj SS Adj MS F-Value P-Value uld direction 40750 40750 40749.8 53.15 0.000  $B_d$ 1 21.87% r thickness 4 46468 24.94% 46468 15.15 0.000  $L_{t}$ 11617.1 4 67867 36.43% 67867 16966.8 22.13 0.000  $I_{t}$ Support angle 4 3614 1.94% 3614 903.4 1.18 0.337 Error 36 27602 14.82% 27602 766.7 Total 49 186301 100.00%

Table 4. Analysis of variance for N.

The regression equation obtained for max force as a result of the analysis is given below.

 $\begin{array}{lll} N=& 396.20+28.55\ B_{d}\_Edge-28.55\ B_{d}\_Upright+38.04\ L_{t}\_0.\\ 09+22.14\ L_{t}\_0.14+2.31\ L_{t}\_0.19-11.85\ L_{t}\_0.29-50.64\\ L_{t}\_0.39+51.13\ I_{t}\_Full-58.84\ I_{t}\_Light+0.57\ I_{t}\_Medium-14.93\ I_{t}\_Mesh+22.08\ I_{t}\_Solid+10.68\ S_{a}\_20-1.00\ S_{a}\_3\\ 0-0.91\ S_{a}\_40-14.56\ S_{a}\_50+5.79\ S_{a}\_60 \end{array}$ 

When the graph in Figure 9 is analyzed, it is observed that the best elongation at break results were obtained at 0.09 mm layer thickness, full infill type and 40° support angle. When the ANOVA values for elongation at break (Table 5) are analyzed, build direction with 25.19%, Layer thickness with 31.70% and Infill type with 38.27% were effective. However, support angle (0.75%) did not show a significant effect on the elongation at break.

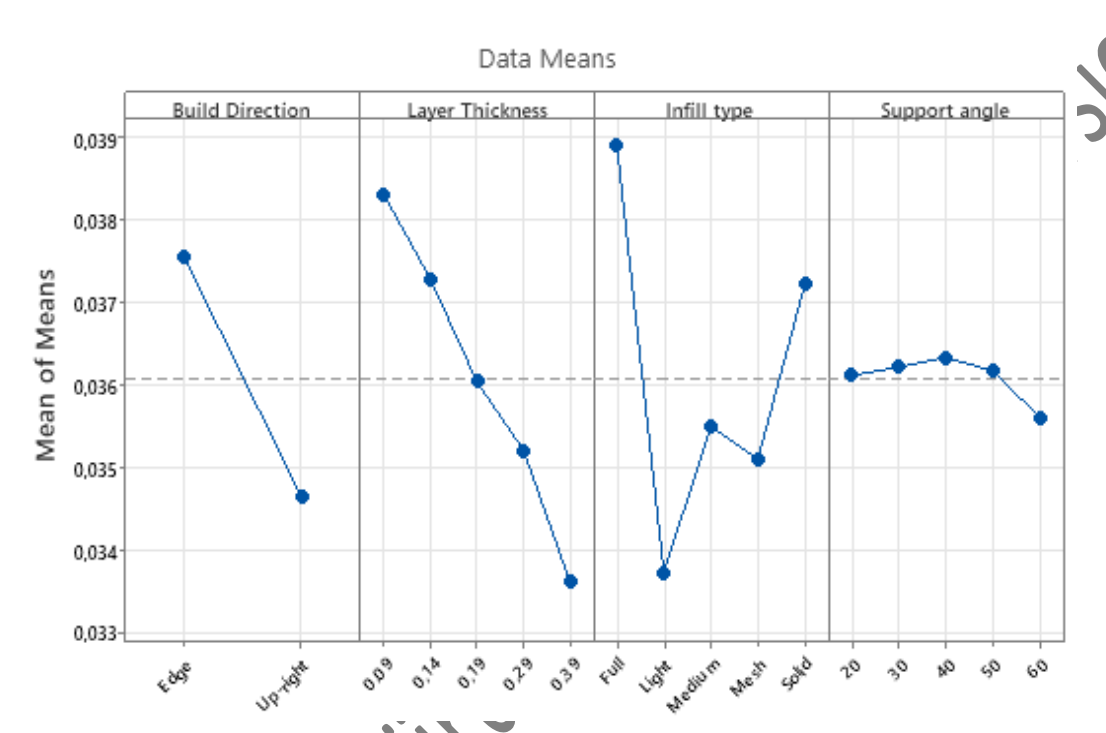


Figure 9. The effects of parameters on elongation at break. Table 5. Analysis of variance for  $\epsilon$ .

Source	DF	Seg SS	Contribution	Adj SS	Adj MS	F-Value	P-Value
Build direction	1	0.000106	25.19%	0.000106	0.000106	221.50	0.000
Layer thickness	4	0.000134	31.70%	0.000134	0.000033	69.69	0.000
Infill type	4	0.000161	38.27%	0.000161	0.000040	84.15	0.000
Support angle	4	0.000003	0.75%	0.000003	0.000001	1.65	0.182
Error	36	0.000017	4.09%	0.000017	0.000000		
Total	49	0.000422	100.00%				

The regression equation obtained for elongation at break as a result of the analysis is given below.

 $\begin{array}{c} 0.036088 + \ 0.001457 \ B_{d\_}Edge\mbox{--}\ 0.001457 \ B_{d\_} \\ Upright\mbox{+-}\ 0.002229 \ L_{t\_}0.09 + \ 0.001195 \ L_{t\_}0.14 \mbox{--} \\ 0.000052 \ L_{t\_}0.19 - \ 0.000885 \ L_{t\_}0.29 - \ 0.002487 \end{array}$ 

 $\begin{array}{l} L_{\rm L}0.39 + 0.002818 \; I_{\rm L}Full \text{--}\; 0.002365 \; I_{\rm L}Light \text{--}\; 0.\\ 000593 \; I_{\rm L}Medium \text{--}\; 0.000988 \; I_{\rm L}Mesh + 0.00112 \\ I_{\rm L}Solid + 0.000028 \; S_{\rm a}\_20 + 0.000125 \; S_{\rm a}\_30 + 0.\\ 000246 \; S_{\rm a}\_40 + 0.000083 \; S_{\rm a}\_50 \text{--}\; 0.000483 \; S_{\rm a}\_60 \end{array}$ 

When the graph in Figure 10 is analyzed, it is observed that the best tensile stress results were obtained at 0.09 mm layer thickness, full infill type and 60° support angle. When the ANOVA values for tensile strength (Table 6) are analyzed, build direction with 42.38%, Layer thickness with 15.16% and Infill type with 37.14% were effective. However, support angle (0.37%) did not show a significant effect on tensile stress.

#### Data Means

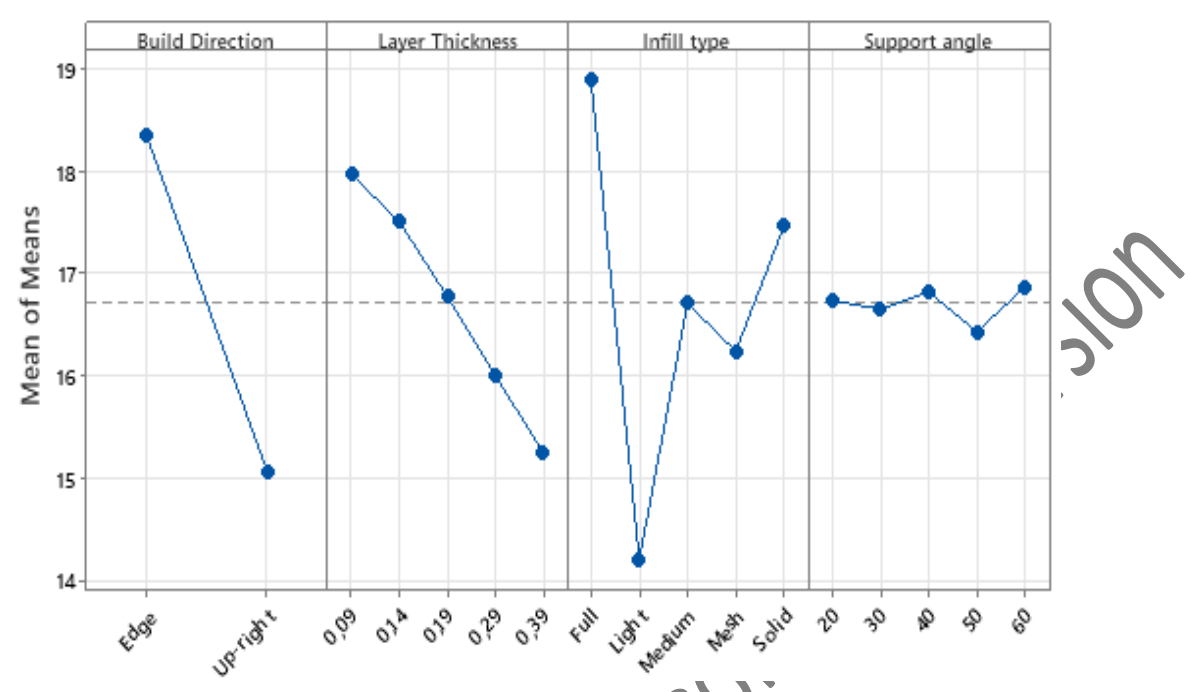


Figure 10. The effects of parameters on tensile strength.

Table 6. Analysis of variance for o.

Source	DF	Seq SS	Contribution	Adj SS	Adj MS	F-Value	P-Value
Build direction	1	134.678	42.38%	134.678	134.678	308.32	0.000
Layer thickness	4	48.171	15.16%	48.171	12.043	27.57	0.000
Infill type	4	118.020	37.14%	118.020	29.505	67.55	0.000
Support angle	4	1.189	0.37%	1.189	0.297	0.68	0.610
Error	36	15.725	4.95%	15.725	0.437		
Total	49	317.783	100.00%				

The regression equation obtained for tensile stress as a result of the analysis is given below.

$$\begin{split} \sigma &= 16.7054 + 1.6412 \; B_{d\_} Edge\text{---} \, 1.6412 \; B_{d\_} Upright + 1.263 \; L_t \\ &= 0.09 + 0.802 \; L_t \, 0.14 + 0.075 \; L_t \, 0.19 - 0.694 \; L_t \, 0.29 - 1.4 \\ &= 46 \; L_t \, 0.39 + 2.190 \; I_t \, Full - 2.494 \; I_t \, Light + 0.005 \; I_t \, Mediu \\ &= 0.459 \; I_t \, Mesh + 0.758 \; I_t \, Solid + 0.036 \; S_a \, 20 - 0.053 \; S_a \\ &= 30 + 0.118 \; S_a \, 40 - 0.270 \; S_a \; 50 + 0.168 \; S_a \, 60 \end{split}$$

The ANOVA values for the effects of the parameters on tensile strength are given in Table 3. According to the table, it was concluded that layer thickness and filler type were highly

effective (P<0.05) on tensile strength. However, support angle had no significant effect on tensile strength.

When the graph in Figure 11 is analyzed, it is observed that the best tensile stress results were obtained at 0.19 mm layer thickness, full infill type and  $60^{\circ}$  support angle. When the ANOVA values for tensile strength (Table 7) are analyzed, build direction with 4.81%, Layer thickness with 2.94% and Infill type with 6.74% were effective. However, support angle (67.68%) did not show a significant effect on tensile stress.

### Main Effects Plot for Means

Data Means

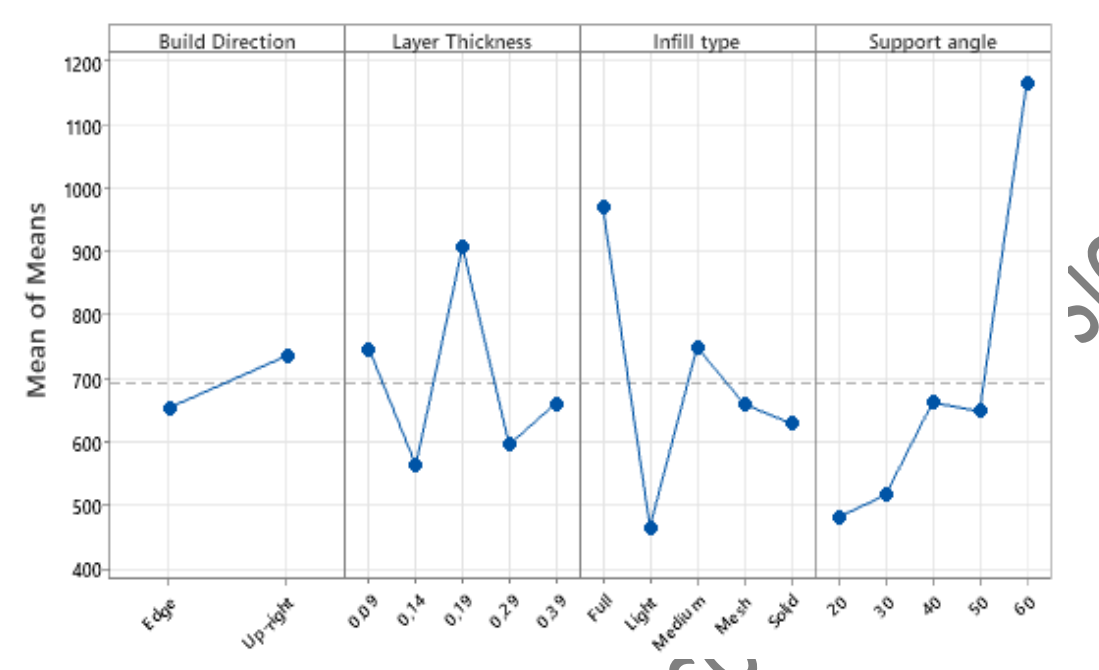


Figure 11. The effects of parameters on elastic modüle. Table 7. Analysis of variance for  $\sigma$ .

Source	DF	Seq SS	Contribution	n Adj SS	Adj MS	F-Value	P-Value
Build direction	1	83953	4,81%	<b>83953</b>	83953	0,18	0,675
Layer thickness	4	761964	2.94%	761964	190491	0,38	0,824
Infill type	4	1362803	6.74%	1362803	340701	0,72	0,580
Support angle	4	2248205	67.68%	2248205	2248205	4,78	0,034
Error	36	1973768	17.83%	19737688	469945		
Total	49	2347256	100.00%				

The regression equation obtained for tensile stress as a result of the analysis is given below.

$$\begin{split} E &= 766 + 0.0 \; L_t \_ 0.09 - 183 \; L_t \_ 0.14 + 161 \; L_t \_ 0.19 - 151 \; L_t \\ &\_ 0.29 - 85 \; L_t \_ 0.39 + 0.0 \; S_a \_ 20 + 35 \; S_a \_ 30 + 181 \; S_a \_ 40 \\ &+ 166 \; S_a \_ 50 + 684 \; S_a \_ 60 + 0.0 \; B_d \_ Edge + 82 \; B_d \_ Upright + 0.0 \; I_t \_ Full - 503 \; I_t \_ Light - 221 \; I_t \_ Medium - 310 \; I_t \_ Mesh - 341 \; I_t \_ Solid \end{split}$$

The results obtained are given in the table 8 below. In general, the models obtained with both linear regression and xgboost and catboost algorithms are quite suitable. For max force, the  $\rm r^2$  value (0.757) was best in Catboost algorithm. Approximate values were also obtained in Linear regression (0,79). For elongation at break, the highest  $\rm r^2$  value (0.906) was obtained in the Catboost algorithm. For tensile strength, the highest  $\rm r^2$  value (0.861) was obtained in the Catboost algorithm. This has demonstrated that catboost is effective, as in similar studies [21]. For elastic module, the highest  $\rm r^2$  value (0.27) was obtained in the xgboost algorithm. However, this situation is not a desirable or expected outcome.

Table 8. Machine learning results

	Linear Regression Xgboost											Catb	boost					
		Test			Train			Test			Train			Test			Train	
	r <sup>2</sup>	rmse	mape	r <sup>2</sup>	rmse	mape	r <sup>2</sup>	rmse	mape	r <sup>2</sup>	rmse	mape	r <sup>2</sup>	rmse	mape	r <sup>2</sup>	rmse	mape
Y1	0.79	26.69	0.062	0.59	34.66	0.076	0.507	30.514	0.058	1.0	0.0048	0.00008	0.757	20.32	0.040	1.0	0.008	0.000016
Y2	0.87	0.001	0.023	0.82	0.001	0.026	0.77	0.001	0.025	0.97	0.0004	0.009	0.906	0.001	0.018	1.0	0.00	0.00001
Y3	0.86	0.95	0.047	0.74	1.17	0.057	0.76	1.11	0.56	1.00	0.0008	0.77	0.861	0.76	0.40	1.0	0.00055	0.000024
Y4	-4.04	201.3	0.309	-5.12	237.1	0.350	0.27	206.48	0.358	1.0	0.0018	0.00003	-1.654	173.99	0.283	1.0	0.125	0.00025

When the max force graphs are analyzed, the blue marks indicate the test results and the orange marks indicate the model values (Figure 12). A consistent and meaningful parallelism is observed here. In addition, in the graphs of Xgboost and Catboost algorithms, test data and model data overlap in places. This is a result of the validity of the model.

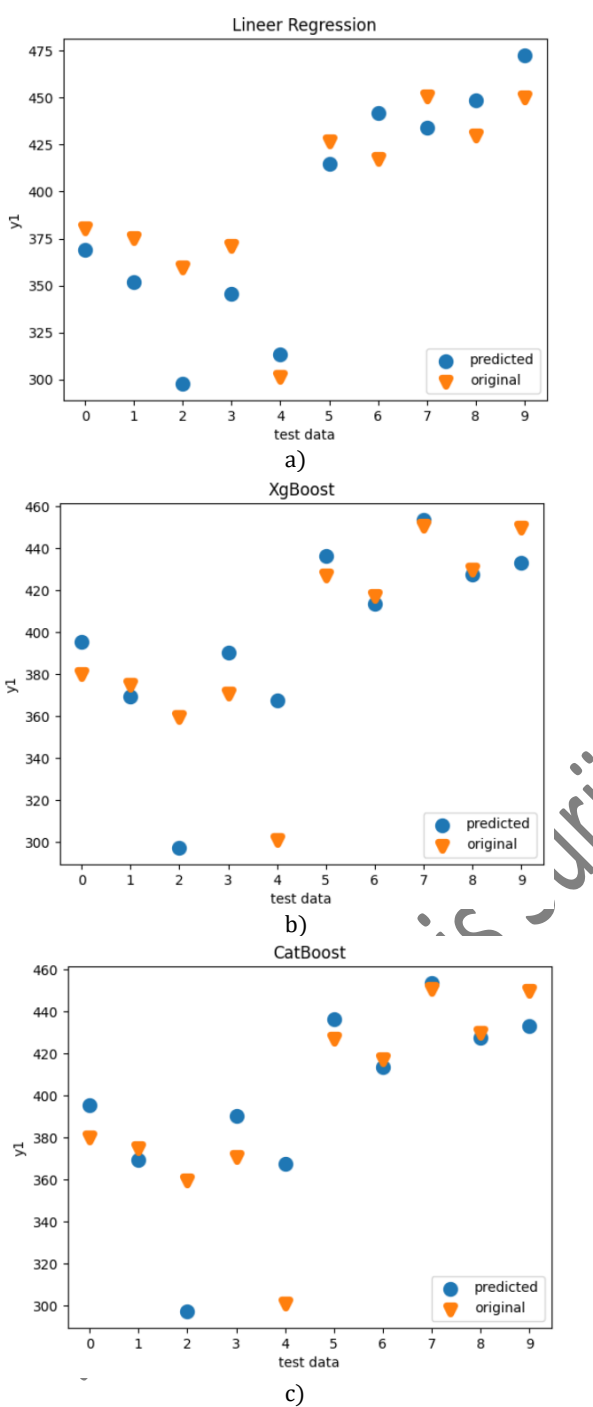


Figure 12. Max force graphs; (a) Lineer regression, (b) Xgboost, (c) Catboost algorithm.

When the elongation at break graphs are analyzed, a consistent and meaningful distribution of linear regression and other Xgboost and Catboost algorithms is observed here (Figure 13). In addition, in the graphs of Linear regression, Xgboost and

Catboost algorithms, test data and model data overlap in places. This is a result of the accuracy of the model.

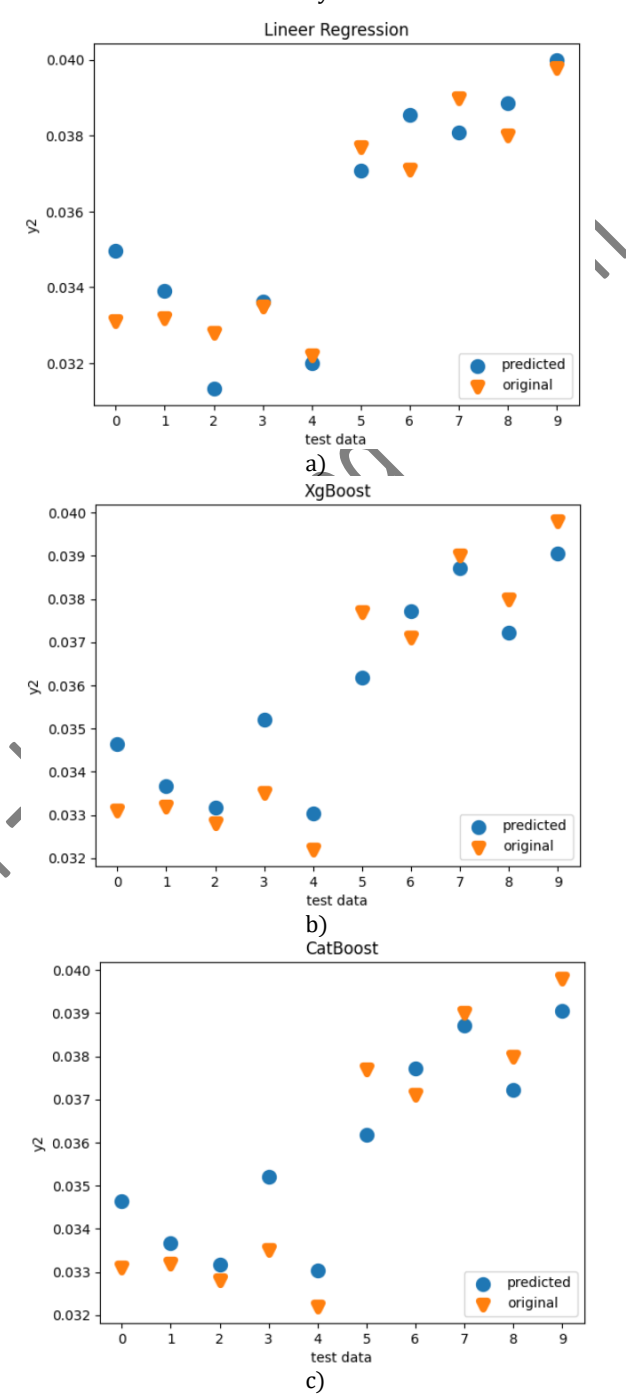


Figure 13. Elongation at break graphs; (a) Lineer regression, (b) Xgboost, (c) Catboost algorithm.

When the tensile strength graphs are analyzed, the model fitting valid for the other two concepts is also observed here (Figure 14). The model obtained with both linear regression and xgboost and catboost algorithms is quite appropriate.

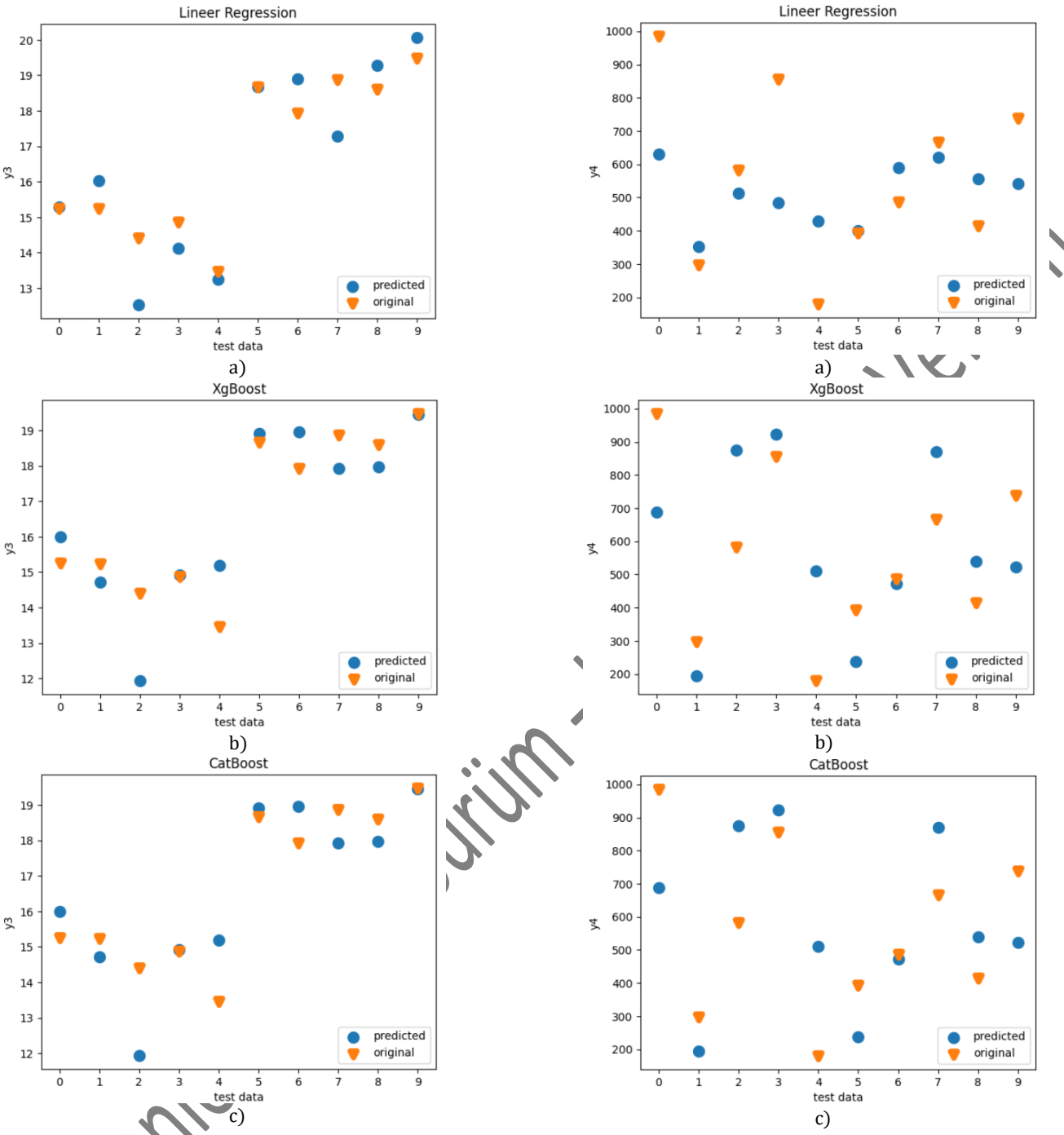


Figure 14. Tensile strength graphs; (a) Lineer regression, (b) Xgboost, (c) Catboost algorithm.

When the elastic module graphs are analyzed, a consistent and meaningful distribution of linear regression and other Xgboost and Catboost algorithms is observed here (Figure 15). However, in the graphs of the linear regression, Xgboost and Catboost algorithms, the test data and model data appear quite distinct. This has been an indication that the model is not as expected and the results are not favourable.

Figure 15. Elastic module; (a) Lineer regression, (b) Xgboost, (c) Catboost algorithm.

According to the results, three validation experiments were conducted (Figure 16). Accordingly, the best maximum force value was obtained with Edge, a layer thickness of 0.09 mm layer thickness, full fill type, and a support value of 20°. The average maximum force value obtained here is 423.56 N. The best elongation at break value was obtained with Edge, 0.09 mm layer thickness, full infill type, and 40° support values. The average elongation at break value obtained here is 0.037. The best tensile strength value was obtained with Edge, 0.09 mm layer thickness, full infill type, and 60° support values. The average tensile strength value obtained here is 16.91MPa. The best elastic modulus value was obtained with Up-right, 0.19

mm layer thickness, full infill type, and  $60^{\circ}$ support values. The average elastic modulus value obtained here is 796.35 MPa.



Figure 16. verification test samples

#### 4 Conclusion

An investigation was conducted into the mechanical properties of prototypes produced using 3D printers with the FDM method. The results of this investigation are presented in the following section.

The optimal layer thickness for achieving maximum force, elongation at break and tensile strength was determined to be 0.09 mm, while the optimum full filler type was identified as well. Furthermore, the investigation revealed that the optimal support angle was  $20^{\circ}$ . With regard to the direction of build, optimal outcomes were achieved at the edge position.

The maximum force value that was recorded was 482 N, while the elongation at break was found to be 0.042 and the tensile strength was determined to be 21.868.

For max force, the  $r^2$  value (0.757) was best in Catboost algorithm. Approximate values were also obtained in Linear regression (0.788). For elongation at break, the highest  $r^2$  value (0.906) was obtained in the Catboost algorithm. For tensile strength, the highest  $r^2$  value (0.861) was obtained in the Catboost algorithm.

As demonstrated by the analysis of variance (ANOVA) results, the build direction, layer thickness and infill type were found to have a significant impact on the maximum force, elongation at break and tensile strength. However, the effect of the support angle was found to be negligible.

#### 5 Author contributions

Author 1 and Author 2, wrote the main manuscript text. All authors reviewed the manuscript.

## 6 Competing interests

There is no need to obtain ethics committee approval for the article prepared. The authors declare no competing interests.

### 7 References

- [1] J. Cantrell vd., "Experimental Characterization of the Mechanical Properties of 3D-Printed ABS and Polycarbonate Parts Nomenclature 3D = Three-dimensional AM = Additive manufacturing ABS = Acrylomitrile butadiene styrene ASTM = American Society for Testing and Materials CA", Proceedings of the 2016 Annual Conference on Experimental and Applied Mechanics, ss. 89–105, 2107.
- [2] A. K. Sood, R. K. Ohdar, ve S. S. Mahapatra, "Parametric appraisal of mechanical property of fused deposition modelling processed parts", *Materials and Design*, c. 31, sayı 1, ss. 287–295, 2010, doi: 10.1016/j.matdes.2009.06.016.
- [3] H. L. Tekinalp *vd.*, "High modulus biocomposites via additive manufacturing: Cellulose nanofibril networks as 'microsponges'", *Composites Part B: Engineering*, c. 173, s. 106817, Eyl. 2014, doi:

- 10.1016/j.compositesb.2019.05.028.
- [4] F. Ning, W. Cong, Y. Hu, ve H. Wang, "Additive manufacturing of carbon fiber-reinforced plastic composites using fused deposition modeling: Effects of process parameters on tensile properties", *Journal of Composite Materials*, c. 51, sayı 4, ss. 451–462, 2017, doi: 10.1177/0021998316646169.
- [5] N. Sa'ude, S. H. Masood, M. Nikzad, ve M. Ibrahim, "Dynamic Mechanical Properties of Copper-ABS Composites for FDM Feedstock", *International Journal of Engineering Research and Applications (IJERA)*, c. 3, sayı 3, ss. 1257–1263, 2013, [Çevrimiçi]. Available at: http://scholar.google.com/scholar?hl=en&btnG=Sear ch&q=intitle:Dynamic+Mechanical+Properties+of+Copper-ABS+Composites+for+FDM+Feedstock#0
- pper-ABS+Composites+for+FDM+Feedstock#0

  S. Bacak, H. Varol Özkavak, ve M. Tath, "FDM Yöntemi ile Üretilen PLA Numunelerin Çekme Özelliklerine İşlem Parametrelerinin Etkisinin İncelenmesi", Mühendislik Bilimleri ve Tasarım Dergisi, c. 9, sayı 1, ss. 209–216, Mar. 2021, doi: 10.21923/jesd.750264.
- [7] H. Evlen, "Doluluk Oranının 3B Yazıcıda Üretilen TPU ve TPE Numunelerinin Mekanik Özellikleri Üzerine Etkilerinin İncelenmesi", *Deu Muhendislik Fakultesi Fen ve Muhendislik, c.* 21, sayı 63, ss. 793–804, 2019, doi: 10.21205/deufmd.2019216310.
- [8] M. Günay, S. Gündüz, H. Yılmaz, N. Yaşar, ve R. Kaçar, PLA Esaslı Numunelerde Çekme Dayanımı İçin 3D Baskı İşlem Parametrelerinin Optimizasyonu", Politeknik Dergisi, c. 23, sayı 1, ss. 73–79, Mar. 2020, doi: 10.2339/politeknik.422795.
- [9] H. K. Sezer, O. Eren, H. R. Börklü, ve V. Özdemir, "karbon fiber takviyeli polimer kompozitlerin ergiyik biriktirme yöntemi ile eklemeli imalatı: fiber oranı ve yazdırma parametrelerinin mekanik özelliklere etkisi", *Gazi Üniversitesi Mühendislik-Mimarlık Fakültesi Dergisi*, c. 2018, sayı 2018, ss. 663–674, Nis. 2018, doi: 10.17341/gazimmfd.416523.
- [10] S. Demir, "The effect of printing parameters on hardness in the production of Poli lactic acid (PLA)-based samples with a 3D printer", *Pamukkale University Journal of Engineering Sciences*, c. 30, sayı 2, ss. 136–144, 2024, doi: 10.5505/pajes.2023.49404.
- [11] I. Malashin, V. Tynchenko, A. Gantimurov, V. Nelyub, ve A. Borodulin, "Boosting-Based Machine Learning Applications in Polymer Science: A Review", *Polymers*, c. 17, sayı 4, ss. 1–42, 2025, doi: 10.3390/polym17040499.
- [12] L. Zhang ve D. Jánošík, "Enhanced short-term load forecasting with hybrid machine learning models: CatBoost and XGBoost approaches", Expert Systems with Applications, c. 241, sayı August 2023, 2024, doi: 10.1016/j.eswa.2023.122686.
- [13] H. Mesghali, B. Akhlaghi, N. Gozalpour, J. Mohammadpour, F. Salehi, ve R. Abbassi, "Predicting maximum pitting corrosion depth in buried transmission pipelines: Insights from tree-based machine learning and identification of influential factors", *Process Safety and Environmental Protection*, c. 187, sayı September 2023, ss. 1269–1285, 2024, doi: 10.1016/j.psep.2024.05.014.
- [14] S. S. Dhaliwal, A. Al Nahid, ve R. Abbas, "Effective intrusion detection system using XGBoost", *Information (Switzerland)*, c. 9, say1 7, 2018, doi:

- 10.3390/info9070149.
- [15] S. Thongsuwan, S. Jaiyen, A. Padcharoen, ve P. Agarwal, "ConvXGB: A new deep learning model for classification problems based on CNN and XGBoost", Nuclear Engineering and Technology, c. 53, sayı 2, ss. 522–531, 2021, doi: 10.1016/j.net.2020.04.008.
- [16] R. Zabin, K. F. Haque, ve A. Abdelgawad, "PredXGBR: A Machine Learning Framework for Short-Term Electrical Load Prediction †", *Electronics (Switzerland)*, c. 13, sayı 22, ss. 1–26, 2024, doi: 10.3390/electronics13224521.
- [17] J. Tian *vd.*, "Synergetic Focal Loss for Imbalanced Classification in Federated XGBoost", *IEEE Transactions on Artificial Intelligence*, c. 5, sayı 2, ss. 647–660, 2024, doi: 10.1109/TAI.2023.3254519.
- [18] S. Alsulamy, "Predicting construction delay risks in Saudi Arabian projects: A comparative analysis of CatBoost, XGBoost, and LGBM", Expert Systems with Applications, c. 268, sayı March 2024, s. 126268, 2025, doi: 10.1016/j.eswa.2024.126268.
- [19] H. Zhuo, T. Li, W. Lu, Q. Zhang, L. Ji, ve J. Li, "Prediction model for spontaneous combustion temperature of coal based on PSO-XGBoost algorithm", Scientific reports, c. 15, sayı 1, s. 2752, 2025, doi: 10.1038/s41598-025-87035-2.
- [20] Y. Ueki, N. Seko, ve Y. Maekawa, "Machine learning approach for prediction of the grafting yield in radiation-induced graft polymerization", *Applied Materials Today*, c. 25, s. 101158, 2021, doi: 10.1016/j.apmt.2021.101158.
- [21] Z. A. Cevik, K. Ozsoy, A. Ercetin, ve G. Sariisik, "Machine Learning-Driven Optimization of Machining Parameters Optimization for Cutting Forces and Surface Roughness in Micro-Milling of AlSi10Mg Produced by Powder Bed Fusion Additive Manufacturing", Applied Sciences (Switzerland), c. 15, sayı 12, ss. 1–23, 2025, doi: 10.3390/app15126553.
- [22] X. Wang, L. Wen, ve R. Chai, "Optimization of Laser Additive Manufacturing Process Based on XGBoost Algorithm", Journal of The Institution of Engineers (India): Series C, c. 105, sayı 6, ss. 1581–1590, 2024, doi: 10.1007/s40032-024-01119-y.
- [23] L. Wang, W. Zhang, Q. Bao, ve Q. Wang, "XGBoost-based failure prediction method for metal additive manufacturing equipment", *Proceedings of the 34th Chinese Control and Decision Conference, CCDC 2022*, ss. 3059–3064, 2022, doi: 10.1109/CCDC55256.2022.10034052.
- [24] S. Rahmani Dabbagh, O. Ozcan, ve S. Tasoglu, "Machine learning-enabled optimization of extrusion-based 3D printing", *Methods*, c. 206, sayı June 2022, ss. 27–40, 2022, doi: 10.1016/j.ymeth.2022.08.002.
  [25] X. Zhu, F. Jiang, C. Guo, Z. Wang, T. Dong, ve H. Li,
- [25] X. Zhu, F. Jiang, C. Guo, Z. Wang, T. Dong, ve H. Li, "Prediction of melt pool shape in additive manufacturing based on machine learning methods", *Optics and Laser Technology*, c. 159, sayı June 2022, s. 108964, 2023, doi: 10.1016/j.optlastec.2022.108964.
- [26] Z. Zhang, Z. Liu, ve D. Wu, "Prediction of melt pool temperature in directed energy deposition using machine learning", *Additive Manufacturing*, c. 37, sayı October 2020, s. 101692, 2021, doi: 10.1016/j.addma.2020.101692.
- [27] Y. Huang, X. Tian, Z. Zheng, D. Li, A. V. Malakhov, ve A. N. Polilov, "Multiscale concurrent design and 3D printing of continuous fiber reinforced thermoplastic

- composites with optimized fiber trajectory and topological structure", *Composite Structures*, c. 285, sayı September 2021, s. 115241, 2022, doi: 10.1016/j.compstruct.2022.115241.
- [28] J. Zhang, C. Yin, Y. Xu, ve S. L. Sing, "Machine learning applications for quality improvement in laser powder bed fusion: A state-of-the-art review", *International Journal of AI for Materials and Design*, c. 1, sayı 1, s. 26, 2024, doi: 10.36922/ijamd.2301.
- [29] D. Veeman, S. Sudharsan, G. J. Surendhar, R. Shanmugam, ve L. Guo, "Machine learning model for predicting the hardness of additively manufactured acrylonitrile butadiene styrene", *Materials Today Communications*, c. 35, sayı March, s. 106147, 2023, doi: 10.1016/j.mtcomm.2023.106147.
- doi: 10.1016/j.mtcomm.2023.106147.

  A. Garg ve K. Tai, "An ensemble approach of machine learning in evaluation of mechanical property of the rapid prototyping fabricated prototype", *Applied Mechanics and Materials*, c. 575, ss. 493–496, 2014, doi: 10.4028/www.scientific.net/AMM.575.493.
- [31] R. Agarwal, J. Singh, ve V. Gupta, "Predicting the compressive strength of additively manufactured PLA-based orthopedic bone screws: A machine learning framework", *Polymer Composites*, c. 43, sayı 8, ss. 5663–5674, 2022, doi: 10.1002/pc.26881.
- [32] J. Zhu vd., "Surface quality prediction and quantitative evaluation of process parameter effects for 3D printing with transfer learning-enhanced gradient-boosting decision trees", Expert Systems with Applications, c. 237, sayı PB, s. 121478, 2024, doi: 10.1016/j.eswa.2023.121478.
- [33] J. M. Barrios ve P. E. Romero, "Decision tree methods for predicting surface roughness in fused deposition modeling parts", *Materials*, c. 12, sayı 16, 2019, doi: 10.3390/ma12162574.
- [34] A. Boschetto, V. Giordano, ve F. Veniali, "Surface roughness prediction in fused deposition modelling by neural networks", *International Journal of Advanced Manufacturing Technology*, c. 67, sayı 9–12, ss. 2727–2742, 2013, doi: 10.1007/s00170-012-4687-x.
- [35] Z. Li, Z. Zhang, J. Shi, ve D. Wu, "Prediction of surface roughness in extrusion-based additive manufacturing with machine learning", *Robotics and Computer-Integrated Manufacturing*, c. 57, sayı October 2018, ss. 488–495, Haz. 2019, doi: 10.1016/j.rcim.2019.01.004.
- [36] N. Hooda, J. S. Chohan, R. Gupta, ve R. Kumar, "Deposition angle prediction of Fused Deposition Modeling process using ensemble machine learning", ISA Transactions, c. 116, ss. 121–128, 2021, doi: 10.1016/j.isatra.2021.01.035.
- [37] A. Douard, C. Grandvallet, F. Pourroy, ve F. Vignat, "An Example of Machine Learning Applied in Additive Manufacturing", *IEEE International Conference on Industrial Engineering and Engineering Management*, c. 2019-December, ss. 1746–1750, 2018, doi: 10.1109/IEEM.2018.8607275.